The Astronomical Journal, 130:1097–1110, 2005 September

THE CENTURY SURVEY GALACTIC HALO PROJECT. II. GLOBAL PROPERTIES AND THE LUMINOSITY FUNCTION OF FIELD BLUE HORIZONTAL BRANCH STARS

Warren R. Brown, Margaret J. Geller, Scott J. Kenyon, and Michael J. Kurtz
Smithsonian Astrophysical Observatory, Harvard-Smithsonian Center for Astrophysics, 60 Garden Street, Cambridge, MA 02138

Carlos Allende Prieto
McDonald Observatory and Department of Astronomy, University of Texas, Austin, TX 78712

Timothy C. Beers
Department of Physics and Astronomy and Joint Institute for Nuclear Astrophysics,
Michigan State University, East Lansing, MI 48824

and

Ronald Wilhelm
Department of Physics, Texas Tech University, Lubbock, TX 79409
Received 2005 March 4; accepted 2005 May 10

ABSTRACT

We discuss a 175 deg^2 spectroscopic survey for blue horizontal branch (BHB) stars in the Galactic halo. We use the Two Micron All Sky Survey (2MASS) and the Sloan Digital Sky Survey (SDSS) to select BHB candidates, and we find that the 2MASS and SDSS color selection is 38% and 50% efficient, respectively, for BHB stars. Our samples include one likely runaway B7 star 6 kpc below the Galactic plane. The global properties of the BHB samples are consistent with membership in the halo population: the median metallicity is $[\mathrm{Fe/H}] = -1.7$, the velocity dispersion is 108 km s^{-1}, and the mean Galactic rotation of the BHB stars 3 kpc $< |z| <$ 15 kpc is -4 ± 30 km s^{-1}. We discuss the theoretical basis of the Preston, Shectman, and Beers M_V-color relation for BHB stars and conclude that the intrinsic shape of the BHB M_V-color relation results from the physics of stars on the horizontal branch. We calculate the luminosity function for the field BHB star samples using the maximum likelihood method of Efstathiou and coworkers, which is unbiased by density variations. The field BHB luminosity function exhibits a steep rise at bright luminosities, a peak between $0.8 < M_V < 1.0$, and a tail at faint luminosities. We compare the field BHB luminosity functions with the luminosity functions derived from 16 different globular cluster BHBs. Kolmogorov-Smirnov tests suggest that field BHB stars and BHB stars in globular clusters share a common distribution of luminosities, with the exception of globular clusters with extended BHBs.

Key words: Galaxy: halo — Galaxy: stellar content — stars: horizontal-branch

Online material: Machine-readable tables

1. INTRODUCTION

Mapping the stellar halo requires objects that are sufficiently luminous to observe at large distances, yet common enough to sample the halo densely. In Brown et al. (2003; hereafter Paper I), we introduced the Century Survey Galactic Halo Project, a photometric and spectroscopic survey from which we selected blue horizontal branch (BHB) stars as probes of the Milky Way halo. BHB stars meet our criteria for tracer samples: they are intrinsically luminous and are quite numerous, with a number density in the halo that exceeds that of RR Lyrae stars by roughly a factor of 10 (Preston et al. 1991). The spectral types of BHB stars are typically around A0, bluer than most competing stellar populations. As a result, candidate BHB stars in the halo are relatively easy to select by broadband colors alone.

In Paper I we described the detailed stellar spectral analysis techniques developed for the Century Survey Galactic Halo Project. In this paper we investigate the mean Galactic rotation, metallicity, and luminosity function of the halo BHB stars in the context of a complementary 175 deg^2 spectroscopic survey. This new survey extends the work of the original Century Survey Galactic Halo Project by making use of two large-area, multipassband imaging surveys: (1) the Two Micron All Sky Survey (2MASS; Cutri et al. 2003) and (2) the Sloan Digital Sky Survey (SDSS; York et al. 2000).

Previous spectroscopic surveys of field BHB stars have identified BHB stars over large (several 10^3 deg^2) areas of sky to shallower depths (Pier 1983; Wilhelm et al. 1999b), or over small ($\sim 10^2$ deg^2) areas of sky to greater depths (Sommer-Larsen et al. 1989; Arnold & Gilmore 1992; Kinman et al. 1994, 2005; Clewley et al. 2004) than the Century Survey Galactic Halo Project. The exception is the recently published sample of 1170 BHB stars observed by the SDSS as misidentified quasars or as filler objects in low-density regions (Sirko et al. 2004a, 2004b). In comparison, our spectroscopic survey of BHB stars is cleanly selected and 100% complete within our color and magnitude selection limits. Combined with the original Century Survey sample, we have 157 spectroscopically identified BHB stars over 239 deg^2 of sky.

In § 2 we describe the sample selection and spectroscopic observations of the new 175 deg^2 region and discuss selection efficiencies for BHB stars. In § 3 we discuss the basis of BHB luminosity-color-metallicity relations and analyze the global kinematic and abundance properties of our BHB samples. In § 4 we calculate the luminosity functions for our field BHB star samples and compare them with luminosity functions derived from

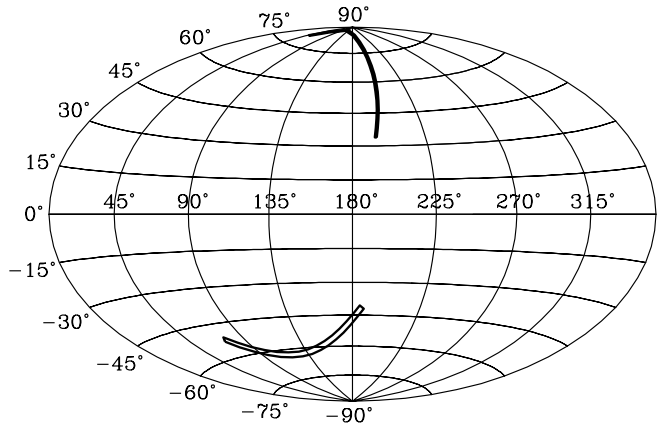

FIG. 1.—Sky map in Galactic coordinates. The Century Survey slice $8^h.5 < \alpha_{B1950} < 13^h.5$, $29^\circ.0 < \delta_{B1950} < 30^\circ.0$, is located in the northern Galactic hemisphere. Our new survey slice, $23^h.0 < \alpha_{J2000} < 3^h.67$, $-1^\circ.25 < \delta_{J2000} < +1^\circ.25$, is located in the southern Galactic hemisphere.

globular cluster data. We summarize our results and conclude in § 5.

2. SAMPLE SELECTION

2.1. *Selection Region*

The original Century Survey Galactic Halo Project contains BHB stars selected by $(V-R)_0$ or $(J-H)_0$ colors. Here we make use only of the sample selected with $(V-R)_0 < 0.3$, the "Century Survey" sample (Brown et al. 2003). The original Century Survey sample covers a $1^\circ \times 64^\circ$ slice located at $8^h.5 < \alpha_{B1950} < 13^h.5$, $29^\circ < \delta_{B1950} < 30^\circ$ and contains 39 spectroscopically confirmed BHB stars in the magnitude range $13 < V_0 < 16.5$.

Here we select BHB candidate stars from the 2MASS and SDSS surveys in a complementary region located along the celestial equator at $23^h0^m0^s < \alpha_{J2000} < 3^h40^m0^s$, $-1^\circ15'0'' < \delta_{J2000} < +1^\circ15'0''$. Figure 1 is a plot of this $70^\circ \times 2^\circ.5$ region in Galactic coordinates. The survey is located predominantly at $b < -45^\circ$, in a region that cleanly samples the halo in the Brown et al. (2004) BHB-candidate maps.

2.2. *2MASS Selection*

The 2MASS catalog provides uniform *JHK* photometry over the entire sky. In Brown et al. (2004), we matched the original Century Survey sample to 2MASS and showed that 2MASS colors select A-type stars with ~80% efficiency. The A-type stars are all good BHB candidates in our high Galactic latitude survey region.

We have selected 90 BHB candidates from the 2MASS catalog in the magnitude range $12.5 < J_0 < 15.5$; BHB candidates have colors in the ranges $-0.2 < (J-H)_0 < 0.1$ and $-0.1 < (H-K)_0 < 0.1$, following Brown et al. (2004). Our upper color limits result in a high selection efficiency but a reduced completeness for BHB stars. Comparison with the original Century Survey sample shows that our color selection samples 65% of the BHB population (Brown et al. 2004).

It is important to note that we have selected objects using dereddened colors and magnitudes, using extinctions from Schlegel et al. (1998). The surface density of the 2MASS-selected BHB candidates is 0.5 deg^{-2}.

We have matched up our 2MASS-selected BHB candidates with the publicly available SDSS data: SDSS photometry presently exists for 65 of the 90 objects. Approximately half of the matched objects have SDSS colors consistent with early A-type stars; the remainder follow the stellar locus to F-type stars (see Fig. 2).

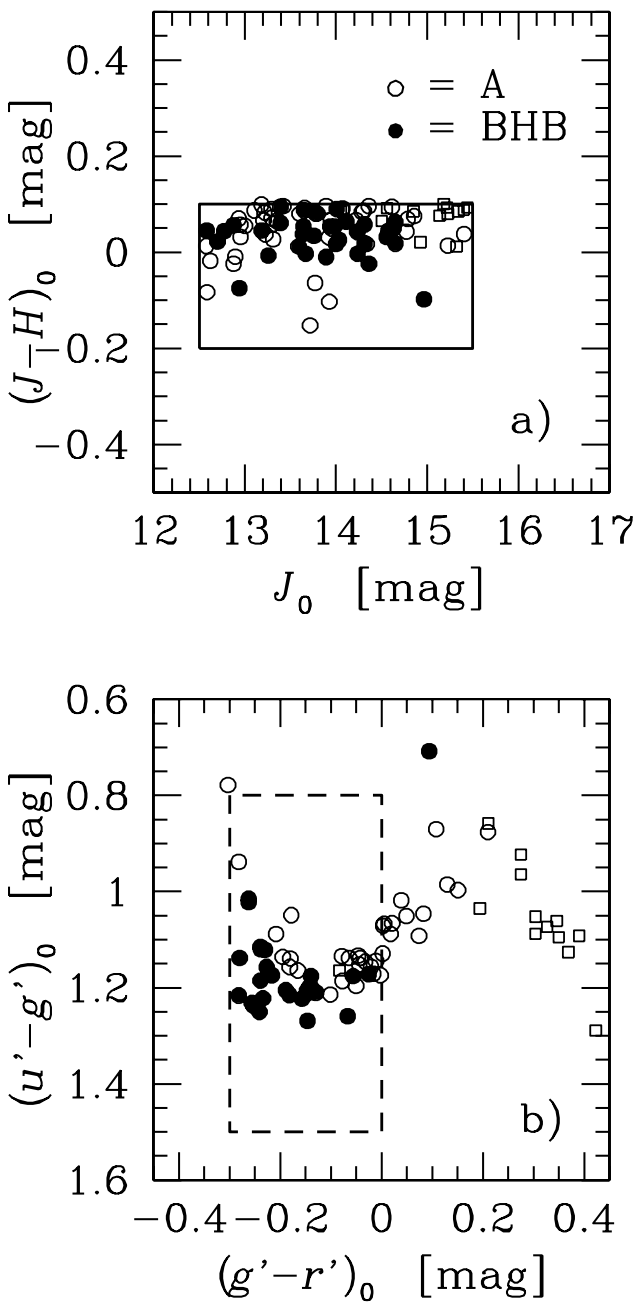

FIG. 2.—The 2MASS-selected BHB candidate sample. (*a*) Distribution of $(J-H)_0$ and J_0; the solid box shows the sample selection region. (*b*) Distribution of $(u'-g')_0$ and $(g'-r')_0$ colors; the dashed box shows the SDSS-sample selection region for comparison. Non-A-type objects are plotted with open squares.

2.3. *SDSS Selection*

The SDSS has released five-passband photometry for limited areas of the sky that can be used to select A-type stars efficiently. We selected 194 BHB candidates in the magnitude range $15 < g'_0 < 17$ from the SDSS Early Data Release (Stoughton et al. 2002) and Data Release 1 (Abazajian et al. 2003). We follow Yanny et al. (2000) and select BHB candidates with $-0.3 < (g'-r')_0 < 0.0$ and $0.8 < (u'-g')_0 < 1.5$. BHB candidates that fall outside the selection box in Figure 3 were objects originally

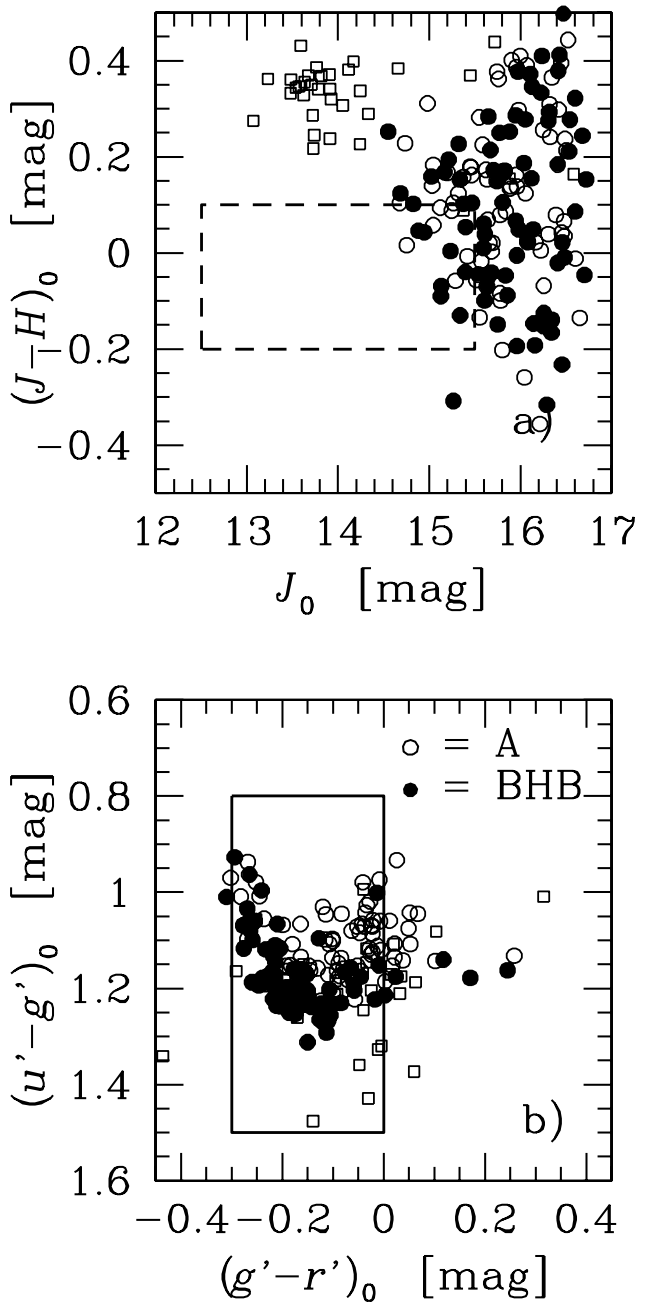

FIG. 3.—Same as Fig. 2, but for the SDSS-selected BHB candidate sample. Objects outside the SDSS-sample selection region (*solid box*) are BHB candidates originally selected by "model" magnitudes from the Early Data Release; here we plot Data Release 1 Petrosian magnitudes that we find are better behaved at bright magnitudes.

selected by "model" magnitudes from the Early Data Release; here we plot Data Release 1 Petrosian magnitudes that we find are better behaved at bright magnitudes. The surface density of the SDSS-selected BHB candidates is 1 deg^{-2}. There is no overlap of these objects with the 2MASS-selected sample, even though both samples cover the same region of sky.

We looked up available 2MASS photometry for the SDSS-selected BHB candidates and found matches for 188 of the 194 objects. A handful of SDSS stars satisfy the 2MASS-selection in J_0 and $(J-H)_0$ but are rejected by $(H-K)_0$. Thus, the lack of overlap between the 2MASS- and SDSS-selected samples is likely due to the extreme uncertainties in 2MASS colors for the fainter 16th and 17th magnitude SDSS stars (see Fig. 3).

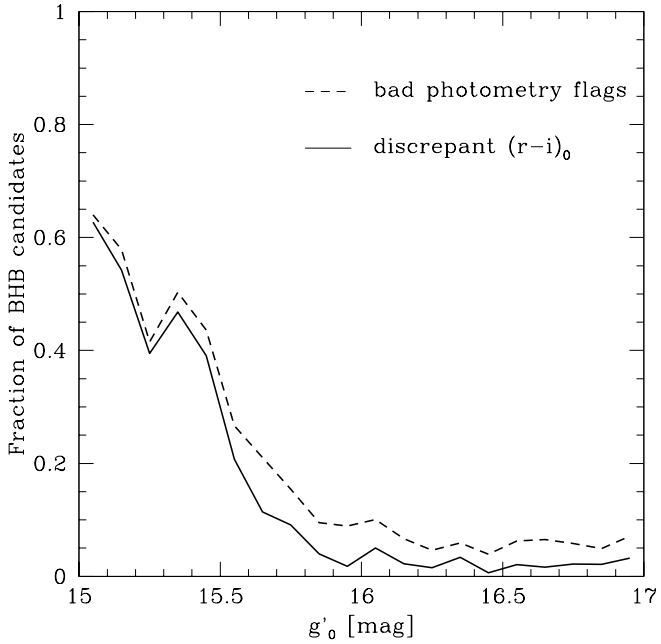

FIG. 4.—Fraction of all A-colored stars in the SDSS DR2 equatorial region with bad photometry flags (*dashed line*) or discrepant $(r'-i')_0 > 0.3$ color (*solid line*).

Interestingly, errant G-type stars found in the SDSS sample are cleanly identified by 2MASS photometry as bright and red $(J-H)_0 \simeq 0.35$ stars. This comparison suggests that some bright (15th to 16th magnitude) SDSS stars are likely saturated and thus have erroneous reported magnitudes. The online documentation for the SDSS data archive now describes a series of flags that can be used to avoid such saturated objects.

To understand our completeness for BHB stars requires a better understanding of the SDSS saturation problem. We start by selecting all stars with A-type colors along the celestial equator in SDSS Data Release 2 (Abazajian et al. 2004). We find that saturated objects have discrepant $(r'-i')_0$ colors for A-type stars. The solid line in Fig. 4 shows the fraction of objects with discrepant $(r'-i')_0 > 0.3$. We then reselect all A-colored stars but this time using the photometry flags to select objects only with clean photometry. The dashed line in Fig. 4 shows the fraction of objects with clean photometry.

Figure 4 shows that half of all A-colored stars with $15 < g'_0 < 15.5$ have erroneous photometry and are not A stars at all. For these objects to have A-type colors in $(u'-g')_0$ and $(g'-r')_0$ but not in $(r'-i')_0$ suggests that the g' band is saturated. This result also suggests that half of the real A-colored stars may be missing in this magnitude range. Selecting for clean photometry removes the erroneous objects but may also reduce the completeness of the sample. The fraction of discrepant A-colored stars drops to $\sim$10% at $g'_0 = 15.75$ (see Fig. 4), and the clean photometry selection maintains this level of apparent incompleteness to $g'_0 = 17$.

2.4. *Spectroscopic Observations*

During the fall 2003 observing season we obtained a spectrum for each BHB candidate in the 2MASS- and SDSS-selected samples. Spectroscopic observations were obtained with the FAST spectrograph (Fabricant et al. 1998) on the Whipple 1.5 m Tillinghast Telescope. We used a 600 lines mm^{-1} grating and a 2″ slit to obtain a resolution of 2.3 Å and a spectral coverage from 3400 to 5400 Å. Typical signal-to-noise ratios (S/N) were 30/1

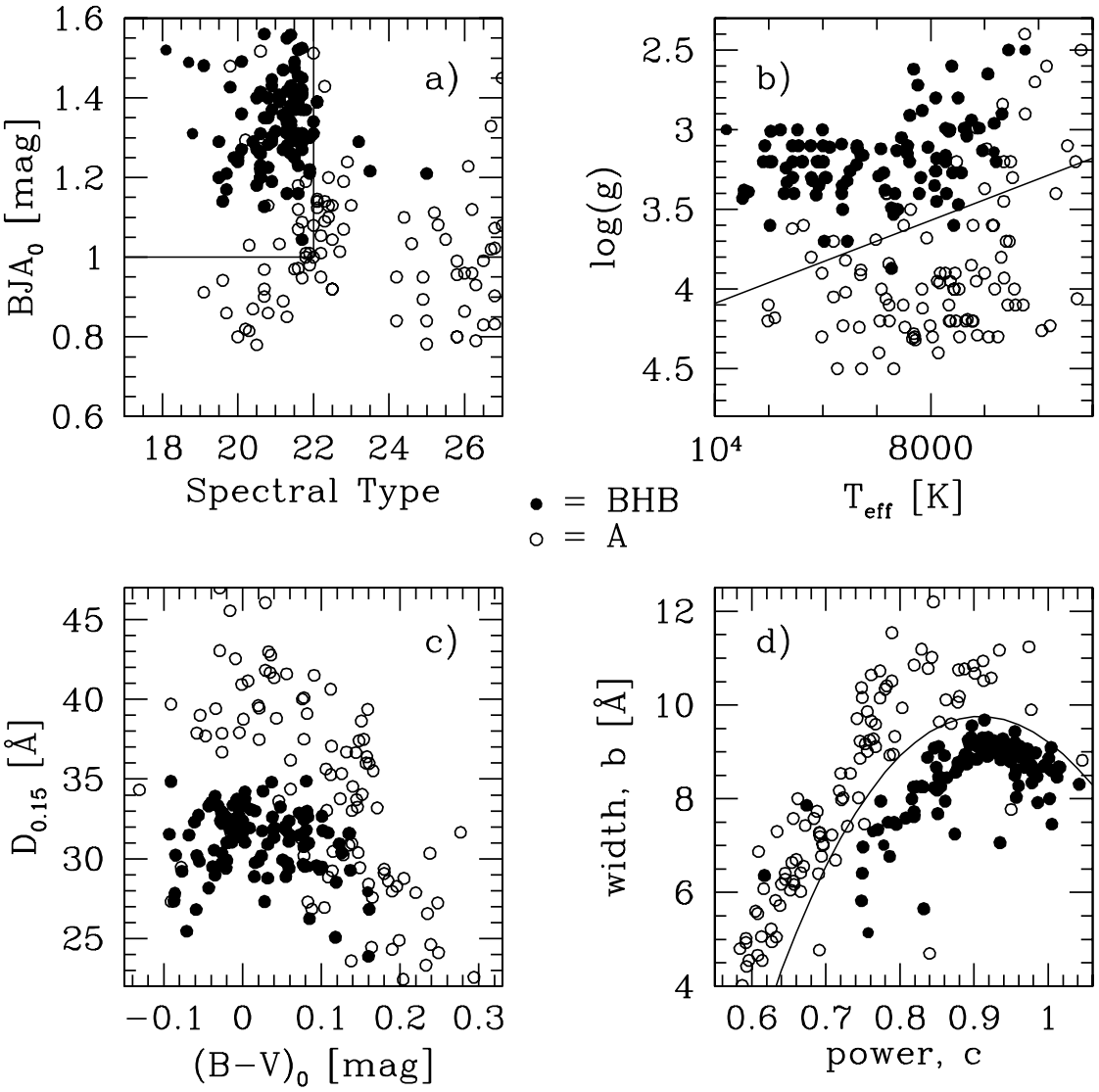

FIG. 5.—Four BHB classification techniques applied to our sample: (*a*) the modified Kinman et al. (1994) method, (*b*) the Wilhelm et al. (1999a) method, (*c*) the Clewley et al. (2002) $D_{0.15}$-color method, and (*d*) the Clewley et al. (2002) scale width-shape method. Filled circles mark the BHB stars; open circles mark the high surface gravity A-type stars.

in the continuum for objects brighter than 16th magnitude, decreasing to S/N = 15/1 for the 17th magnitude objects. This S/N is adequate to measure the Balmer lines and the Balmer jump, which are the primary surface gravity indicators we employ for BHB stars. Paper I contains details of the data reduction. We measure spectral types and radial velocities and derive metallicities, effective temperatures, and surface gravities from the spectra of the total sample of 284 objects.

2.5. *BHB Classification*

The major difficulty in using BHB stars as probes of Galactic structure is the need to distinguish reliably between low surface gravity BHB stars and higher surface gravity A-type dwarfs and blue stragglers. Although investigators once thought blue stragglers were a minor component of the halo population, recent studies (Norris & Hawkins 1991; Preston et al. 1994; Wilhelm et al. 1999b; Brown et al. 2003; Clewley et al. 2004) demonstrate that a surprisingly large fraction of faint stars in the color range associated with BHB stars are indeed high-gravity stars, many of which are blue stragglers (Preston & Sneden 2000; Carney et al. 2005).

Our classification of BHB stars is identical to the approach described in Paper I. In brief, we apply the techniques of Kinman et al. (1994), Wilhelm et al. (1999a), and Clewley et al. (2002) to identify low surface gravity BHB stars. We identify objects that satisfy three or more of the four classification techniques as BHB stars (see Fig. 5). We find a total of 118 BHB stars across our 175 deg^2 survey region.

2.6. *Sample Selection Efficiencies*

Table 1 summarizes sample selection efficiencies. The 2MASS-selected sample contains 34 BHB stars (out of 90 candidates) for a net selection efficiency of 38%. The total number of A-type stars is about twice the number of BHB stars, or 78% of the 2MASS-selected sample. Of the remaining non-A-type objects, 7% of the stars in the 2MASS-selected sample are B-type stars; 15% of the stars in this sample are F-type stars.

The SDSS-selected sample contains 84 BHB stars (out of 167 candidates) for a net selection efficiency of 50%. We ignore the 27 G-type stars in this calculation, as these stars can presumably be rejected by saturation flags. The total number of A-type stars is about twice the number of BHB stars, or 92%

TABLE 1
SELECTION EFFICIENCIES

Sample	N_{stars}	BHB (%)	Other A-type (%)	B-type (%)	F-type (%)
2MASS.....	90	38	40	7	15
SDSS.....	167	50	42	4	4

of the SDSS-selected sample (excluding the G-types). Of the remaining non-A-type objects, 4% of the stars in the SDSS-selected sample are B-type stars; 4% of the stars in this sample are F-type stars.

Sirko et al. (2004a) have recently published a "stringent" color selection for BHB stars. Applying the stringent color cut to our full SDSS-selected sample would yield 55 BHB stars selected from 81 candidates for a net selection efficiency of 68% but a completeness of only 65% compared to the full SDSS-selected sample.

2.7. *Unusual Objects*

In Paper I we identified a number of unusual objects, including white dwarfs, subdwarfs, and B-type stars, within our survey of blue stars in the halo. The 2MASS- and SDSS-selected samples, by comparison, contain a handful of B stars but do not include any white dwarfs or subdwarfs. The lack of white dwarfs may be explained by the more restrictive color selection we used for the 2MASS- and SDSS-selected samples. Moreover, the B-type stars in the 2MASS- and SDSS-selected samples are almost entirely late B8 and B9 stars. These late B-type stars are potentially all hot horizontal-branch stars but are very difficult to classify because the horizontal branch crosses the main sequence at this location in the H-R diagram.

The earliest B-type star in our samples is CHSS 1645, classified as B7. As the earliest B-type star in our samples, CHSS 1645 is the most likely object to be a true B star rather than a hot horizontal-branch star. Assuming CHSS 1645 has solar metallicity, with $M_V \sim -0.6$ (Cox 2000) and $(V-J) = -0.3$ (Kenyon & Hartmann 1995), we estimate that it is located 6 kpc below the Galactic plane. This places CHSS 1645 among the class of stars known as "runaway B-type" stars. The star CHSS 1645 is located at $b = -60^\circ$, hence its +73 km s^{-1} radial velocity points predominantly in the negative z-direction perpendicular to the plane of the Galaxy. If its radial velocity is the majority of its full space motion, it takes 10^8 yr for CHSS 1645 to travel 6 kpc from the Galactic plane. A B7 star has $\sim 4\ M_\odot$ (Cox 2000) and a lifetime $\sim 2 \times 10^8$ yr (Bowers & Deeming 1984). Thus, CHSS 1645, a likely runaway B7 star, has a lifetime consistent with its travel time from the disk.

3. GLOBAL PROPERTIES

To map the Galactic halo requires knowing the intrinsic luminosities of BHB stars. BHB stars are standard candles with luminosities that depend on effective temperature (color) as well as metallicity. We begin by discussing the physical basis of the BHB luminosity dependence on color (§ 3.1). We then present the observed distribution of metallicities derived from our spectra (§ 3.2). Using our colors and metallicities, we compute intrinsic luminosities for our field BHB stars and investigate their spatial distribution (§ 3.3). Finally, we investigate the mean Galactic rotation of our halo samples (§ 3.4).

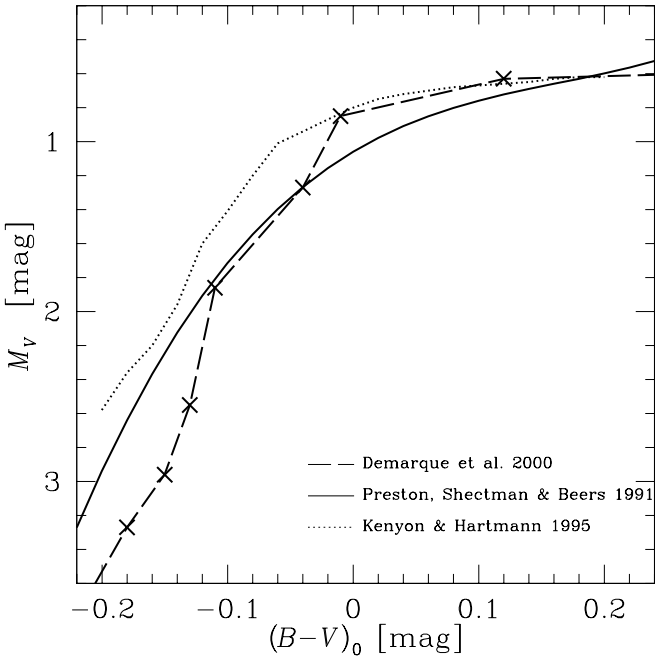

FIG. 6.—BHB M_V-color relations. The solid line shows the empirical Preston et al. (1991) relation derived from globular clusters, the dashed line shows the theoretical relation derived from the Demarque et al. (2000) stellar models, and the dotted line shows our toy model of bolometric corrections (Kenyon & Hartmann 1995) for a constant-luminosity star.

3.1. *BHB Luminosity-Color Dependence*

BHB stars share a common physical origin. They are stars that have evolved off the red giant branch and are burning helium in their cores with a hydrogen-burning shell. The bolometric luminosity of a BHB star depends on the core mass, the stellar mass, and the metallicity (e.g., Demarque et al. 2000). More massive BHB stars have larger hydrogen-rich envelopes and are cooler than less massive BHB stars. The variation of effective temperature with stellar mass yields a robust relation between optical luminosity and $B-V$ color: blue BHB stars are fainter than red BHB stars.

Preston et al. (1991; hereafter PSB91) provide an empirical BHB luminosity-color relation from a fit to 15 globular cluster BHBs. Figure 6 shows the PSB91 M_V-color relation as a solid line. The relation is normalized to $[\mathrm{Fe/H}] = -2.3$ using the M_V-metallicity relation described below. Globular clusters exhibit a wide range of BHB morphologies, evident in the 0.25 mag scatter of the points in PSB91's Figure 5. Because the large scatter may result from the physics of globular clusters rather than from the physics of BHB stars, we next consider a theoretical M_V-color relation. The theoretical M_V-color relation provides a physical basis for the empirical PSB91 relation.

To construct a theoretical M_V-color relation, we use the horizontal-branch evolutionary tracks from Demarque et al. (2000). For models with $Z = 10^{-4}$ (equivalent to $[\mathrm{Fe/H}] = -2.3$) we adopt the luminosity at time zero and derive colors and bolometric temperatures from published tables (Kenyon & Hartmann 1995; Green et al. 1987; Lejeune et al. 1998). The resulting M_V-color relation for $Z = 10^{-4}$ is the dashed line in Figure 6. The theoretical M_V-color relation is remarkably similar in shape to the empirical PSB91 relation in the $(B-V)_0 > -0.1$ region covered by our BHB star samples.

As a consistency check, we plot a third line in Figure 6 that is simply the bolometric correction for a star with constant

luminosity. We use the bolometric corrections for main-sequence stars from Kenyon & Hartmann (1995) and add 0.5 mag to match the bolometric correction to the empirical and theoretical M_V-color relations at the red end. Interestingly, the shape of the Kenyon & Hartmann (1995) bolometric corrections is similar to both the empirical and theoretical BHB M_V-color relations except that the slope of the bolometric correction curve is too shallow at the blue end. We expect this systematic difference, because blue BHB stars are intrinsically less luminous than red BHB stars; we have assumed a constant-luminosity star. Bolometric corrections from Green et al. (1987) and Lejeune et al. (1998) yield similar results, with a typical scatter of 0.1–0.2 mag. This toy model shows that the primary ingredient in the BHB M_V-color relation is the bolometric correction for BHB stars.

Thus, the physics common to all BHB stars leads to a general BHB M_V-color relation, albeit with an intrinsic spread resulting from age and metallicity. The M_V-color relation depends on age, because the luminosity and effective temperature of a BHB star evolve with time. The M_V-color relation has a well-known dependence on metallicity, but Demarque et al. (2000) argue for an additional spread in M_V at a given metallicity due to BHB morphology. The morphology effect is strongest for a metal-poor [Fe/H] < -2 BHB with blue morphology (HB type index $= +1$). According to Demarque et al. (2000), a metal-poor, blue BHB is actually $\sim$0.1 mag brighter than the standard luminosity-metallicity relation predicts. We conclude that the BHB M_V-color relation has an *intrinsic shape* due to the physics of the horizontal branch, with an intrinsic spread of 0.1–0.2 mag. For purposes of discussion, we use the empirical PSB91 M_V-color relation to estimate BHB luminosities in §§ 3.2–3.4.

3.2. *Metallicities*

We measure metallicities for BHB stars as described in Paper I. We use three different techniques: the line indices of Beers et al. (1999), the equivalent width of Ca II K plus a χ^2 comparison between metallic line regions in synthetic and observed spectra (Wilhelm et al. 1999a), and an optimization method that fits the entire spectrum (Allende Prieto 2003). The three techniques are in good agreement with 0.25 dex uncertainty (Brown et al. 2003). The final metallicity is the average of the three techniques; we adopt $\pm$0.25 dex as the error in the final metallicity.

Figure 7 plots the observed distribution of metallicities we measure in the original Century Survey sample, the 2MASS-selected sample, and the SDSS-selected sample. The median [Fe/H] of the BHB samples are indicated by the dashed lines in Figure 7 and range from [Fe/H] $= -1.47$ to -1.75. Our metallicity-measuring techniques are limited to the range $-3 <$ [Fe/H] < 0, and so peaks in Figure 7 at [Fe/H] $= -3$ and 0 are likely stars with lower or higher metallicities piling up at the limits. We caution that the distributions in Figure 7 are the observed and not the intrinsic distributions; because BHB luminosities have a mild dependence on metallicity, stars of different [Fe/H] are sampled from different volumes of space (see below). However, it is clear that our BHB samples are predominantly metal-poor and therefore consistent with a halo population.

A Kolmogorov-Smirnov (K-S) two-sample test provides a simple way to evaluate whether the different BHB samples are drawn from a common parent distribution of [Fe/H]. The K-S two-sample test works by sorting an observed quantity, such as metallicity, and then comparing the cumulative distributions of two different samples with one another. The likelihood is calculated for the null hypothesis that the two distributions are drawn from the same parent distribution. We test the metallicity distributions in Figure 7 in a pairwise fashion and find likelihood values ranging from 14% to 60%. Thus, our BHB samples are consistent with the null hypothesis that the metallicity distributions come from the same (halo) population.

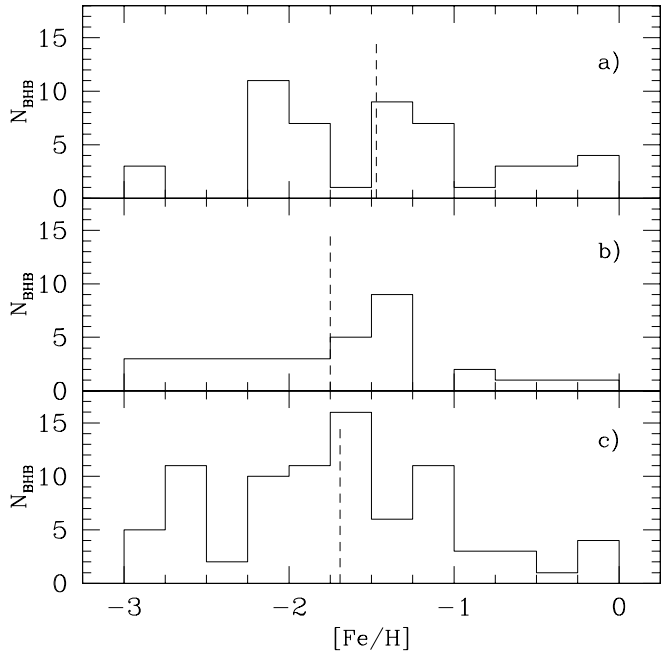

FIG. 7.—Distribution of BHB [Fe/H] for (*a*) the Century Survey sample, (*b*) the 2MASS-selected sample, and (*c*) the SDSS-selected sample. Dashed lines indicate the median [Fe/H]. The error in [Fe/H] is 0.25 dex, the same size as our bins.

3.3. *Spatial Distribution*

We calculate luminosities for our field BHB stars using the M_V(BHB) relation from Clewley et al. (2004). This relation assumes the *Hipparcos*-derived zero point, $M_V(\mathrm{RR}) = 0.77 \pm 0.13$ at [Fe/H] $= -1.60$ (Gould & Popowski 1998), a M_V-metallicity slope 0.214 ± 0.047 based on RR Lyrae stars in the Large Magellanic Cloud (Clementini et al. 2003), and the PSB91 cubic relation in $(B-V)_0$ to provide the temperature correction. Although the PSB91 M_V-color relation was derived for globular cluster BHB stars, the *shape* of the relation reflects the physics common to all BHB stars, as explained above. Note that we do not measure $(B-V)_0$ directly. For the SDSS sample, we are able to make accurate estimates of $(B-V)_0$ from SDSS colors. For the 2MASS sample, we use 2MASS photometry and Balmer line strengths to estimate $(B-V)_0$ as described in Paper I. We refer to these $(B-V)_0$ estimates as $BV0$. From the derived luminosities we compute distances. We expect the relative distances of our BHB stars have a precision of $\sim$6%.

Because the luminosity of a BHB star is dependent on metallicity, the depths reached by our flux-limited samples are dependent on metallicity. Figure 8 shows the distribution of [Fe/H] for the 2MASS- and SDSS-selected samples as a function of z, the distance above or below the Galactic plane. The dotted lines represent the magnitude limits for a BHB star at the median Galactic latitude $b = -57^\circ$ and at the median color $BV0 = 0.03$ of our samples. Metal-rich BHB stars are intrinsically fainter than metal-poor BHB stars. Figure 8 shows that we sample BHB stars with [Fe/H] $= -1$ to 82% of the depth of BHB stars with [Fe/H] $= -3$.

The BHB luminosity dependence on color is stronger than the dependence on metallicity. Thus, there is a strong selection bias with stellar color. In Figure 9 we plot the distribution of $BV0$

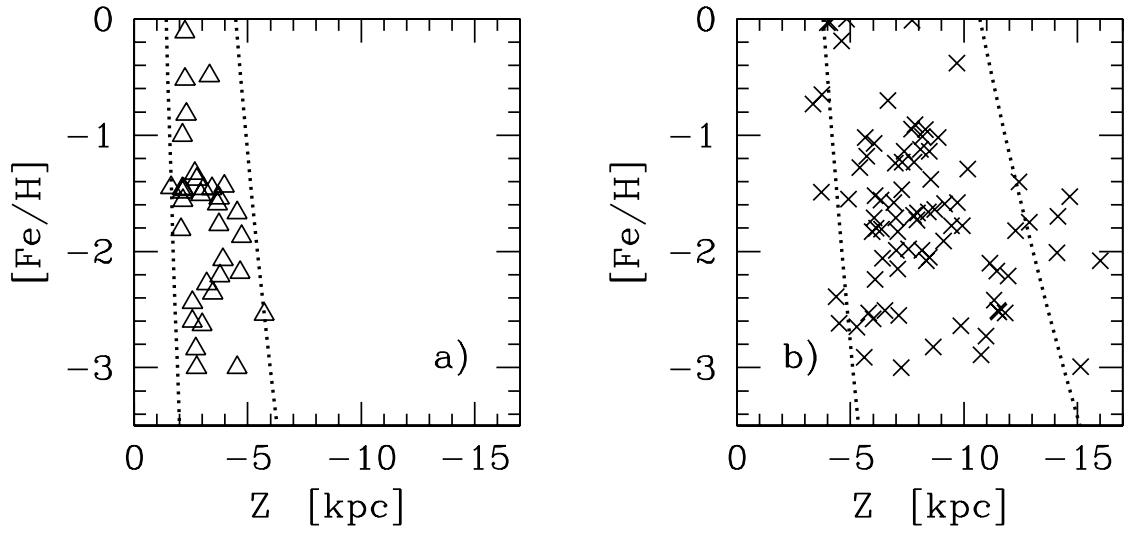

FIG. 8.—Distribution of [Fe/H] vs. z for (a) the 2MASS- and (b) the SDSS-selected samples. The dotted lines represent the magnitude limits for a BHB star at the median Galactic latitude $b = -57^\circ$ and at the median color $BV0 = 0.03$ of the samples. Some stars fall beyond the "limits" because there is a spread of Galactic latitude and color in our samples.

color for the 2MASS- and SDSS-selected samples as a function of z. The dotted lines represent the magnitude limits for a BHB star at the median Galactic latitude $b = -57^\circ$ and at the median metallicity [Fe/H] $= -1.7$ of our samples. Figure 9 shows that we sample BHB stars with $BV0 = -0.1$ to only 64% of the depth that we detect BHB stars with $BV0 = +0.1$. The intrinsically faintest BHB stars are the bluest BHB stars hooking down off the horizontal branch in an H-R diagram. These faint BHB stars are sampled in a smaller volume than the more luminous BHB stars in our samples.

We now plot the spatial distribution of the original Century Survey, the 2MASS-selected, and the SDSS-selected BHB samples (Fig. 10). Spatial distribution is traditionally displayed in a wedge plot for survey slices like ours. However, a wedge plot is inappropriate in the context of the Galaxy, where a slice in celestial coordinates cuts across varying Galactic latitudes. The density of halo and disk populations is a strong function of both R, the distance along the Galactic plane, and z (e.g., Siegel et al. 2002). Thus, in Figure 10 we plot the distribution of BHB stars as a function of R and z. Indeed, the observed distribution of BHB stars clearly depends on both R and z.

The 2MASS- and SDSS-selected BHB candidates sample complementary ranges of distances, but the overlap is unfortunately minimal. The 2MASS and SDSS catalogs formally overlap between 15 and 15.5 mag. However, in this magnitude range, the 2MASS BHB selection suffers from incompleteness due to large color errors and the SDSS BHB selection likely suffers from incompleteness due to saturation problems.

3.4. *Mean Galactic Rotation*

There is wide disagreement in the literature on whether the stellar halo rotates significantly. Previous surveys have found evidence for (1) no halo rotation (Layden et al. 1996; Gould & Popowski 1998; Martin & Morrison 1998; Gilmore et al. 2002; Sirko et al. 2004b), (2) a small prograde rotation (Chiba & Beers 2000), and (3) retrograde rotation (Majewski 1992; Majewski

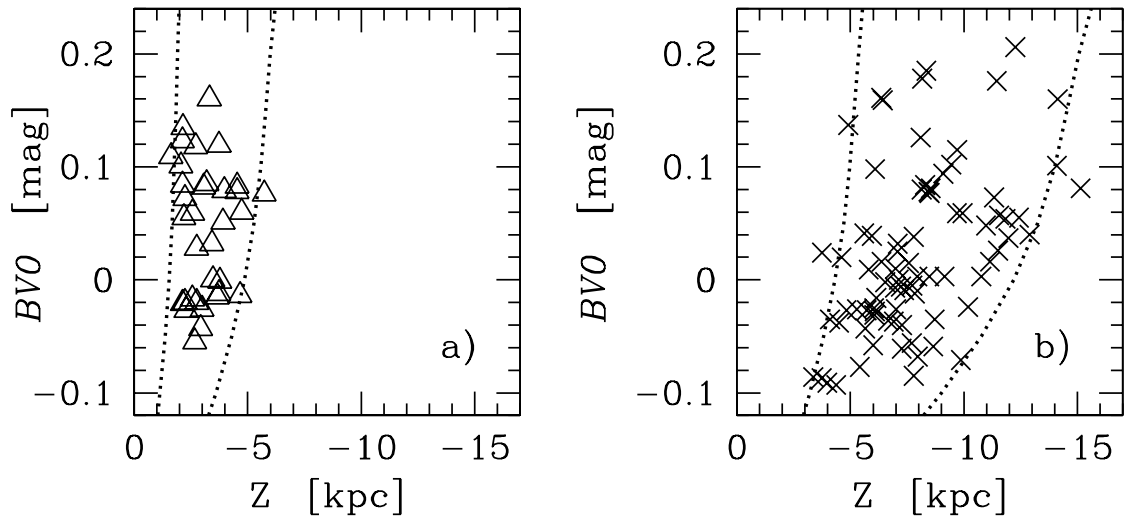

FIG. 9.—Distribution of $BV0$ vs. z for (a) the 2MASS- and (b) the SDSS-selected samples. The dotted lines represent the magnitude limits for a BHB star at the median Galactic latitude $b = -57^\circ$ and at the median metallicity [Fe/H] $= -1.7$ of the samples. Some stars fall beyond the "limits" because there is a spread of Galactic latitude and metallicity in our samples.

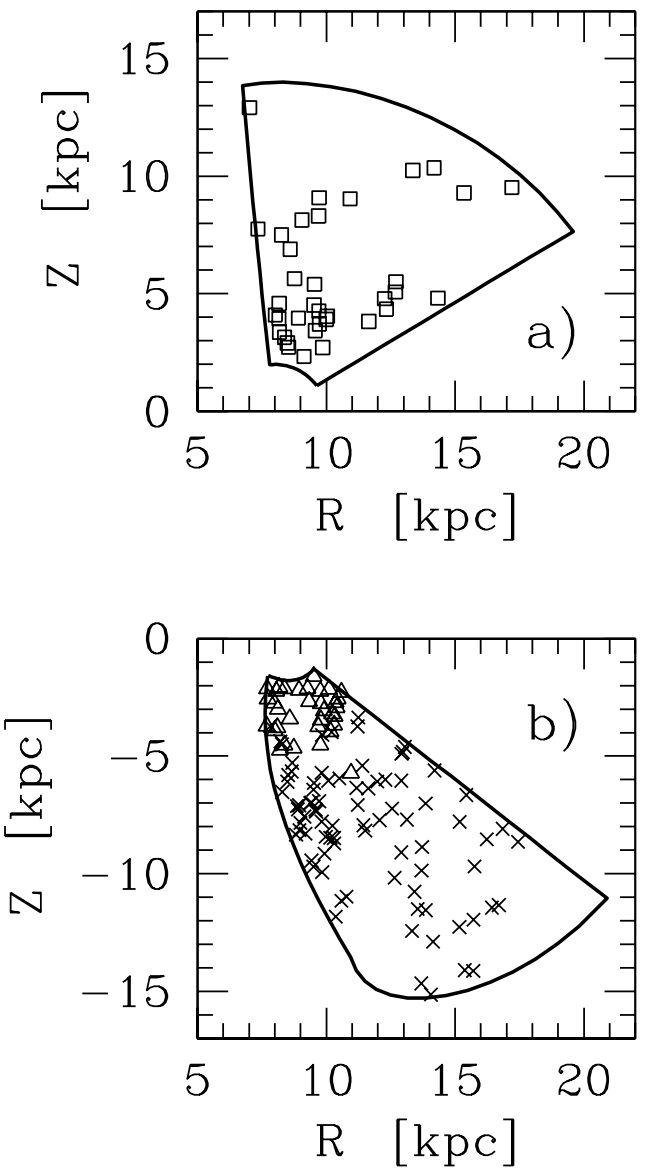

FIG. 10.—Distribution of BHB stars in distance from the Galactic center along the Galactic plane, R, and distance above or below the Galactic plane, z. (*a*) BHB stars in the original Century Survey slice. (*b*) BHB stars in the 2MASS-selected (*triangles*) and SDSS-selected (*crosses*) samples. The solid lines indicate heliocentric distance limits of 2 kpc and (*a*) 14 kpc or (*b*) 17 kpc.

et al. 1996; Spagna et al. 2003; Kinman et al. 2005). Interestingly, all the measurements of retrograde rotation come from surveys of the north Galactic pole. By comparison, the measurements of no rotation come from surveys covering many directions in the sky.

Our BHB samples cover a wide range of Galactic latitude and longitude and so provide us with a reasonably fair sample of the halo. Although high Galactic latitude stars are not ideal for measuring the rotation of the stellar halo, the 2MASS- and SDSS-selected samples include a number of stars near $l \sim 90^\circ$ that are sensitive to a systematic rotation of the halo.

Figure 11 shows the mean rotation velocity of the 2MASS- and SDSS-selected BHB stars as a function of z. Each bin includes $\sim$25 BHB stars that are first corrected to the local standard of rest (Dehnen & Binney 1998) and then evaluated by the methodology of Frenk & White (1980). We assume a solar rotation of 220 km s^{-1}. We expect some contamination from the

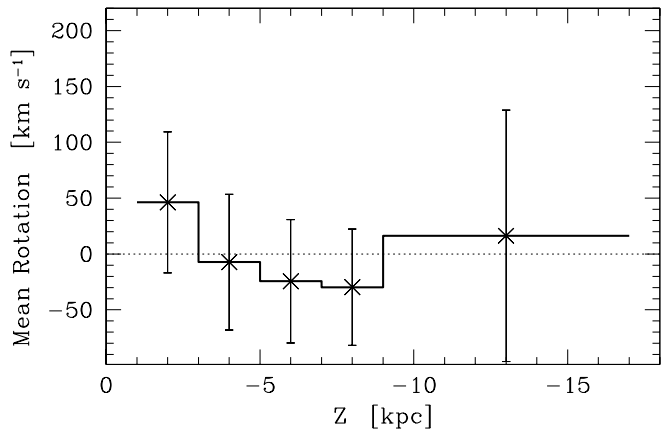

FIG. 11.—Galactic rotation velocity of the 2MASS- and SDSS-selected BHB stars, binned by distance below the Galactic plane, z.

thick disk in the nearest BHB stars, and indeed there is a hint of prograde rotation in the 1 kpc $< |z| <$ 3 kpc bin. The mean rotation velocities of the 3 kpc $< |z| <$ 15 kpc stars are, however, consistent with no rotation. The rotation velocity of the combined sample of 2MASS- and SDSS-selected BHB stars is -4 ± 30 km s^{-1}. The velocity dispersion of the BHB stars is 108 km s^{-1}, also consistent with a halo population.

The BHB stars from the original Century Survey sample cover a similar range of z. However, the Century Survey BHB stars are located toward the Galactic anticenter $l \sim 200^\circ$ and toward the north Galactic pole $b \gtrsim 60^\circ$. Thus, the Century Survey stars provide very little leverage on halo rotation. When we include the Century Survey stars in the mean rotation velocity calculation, we find they add $\sim$10 km s^{-1} of retrograde rotation to the bins. We conclude the mean rotation velocities remain fully consistent with no halo rotation within their errors.

4. THE LUMINOSITY FUNCTION OF BHB STARS

Knowledge of the intrinsic distribution of luminosities of field BHB stars is important for interpreting maps of the Galactic halo. Knowledge of the luminosity function is also important for understanding the intrinsic properties of field BHB stars that cover a broad range of observed magnitude, color, and metallicity. The luminosity function describes the number of stars per unit volume in the luminosity interval L to $L + dL$. We describe the method we use to calculate the BHB luminosity function (§ 4.1) and discuss the role of the M_V-color relation in our result (§ 4.2). We compare the luminosity function we determine for our field BHB stars (§ 4.3) with luminosity functions derived from globular clusters with BHBs (§ 4.4).

4.1. *Calculating the Luminosity Function*

We calculate the luminosity function of our field BHB stars using the nonparametric maximum likelihood method of Efstathiou et al. (1988). The Efstathiou et al. (1988) maximum likelihood method is commonly used to calculate the luminosity function of galaxies in galaxy redshift surveys. We now apply this method to our survey of BHB stars in the Galactic halo. The method does not simply count the numbers of stars at different luminosities but weights the contribution of each star by the relative volume in which it can be observed in a flux-limited sample. Specifically, the probability of a star at distance d falling into the luminosity range $[L, L + dL]$ is equal to the luminosity function at L divided by the number density of stars one expects to see in a flux-limited survey at distance d. The maximum

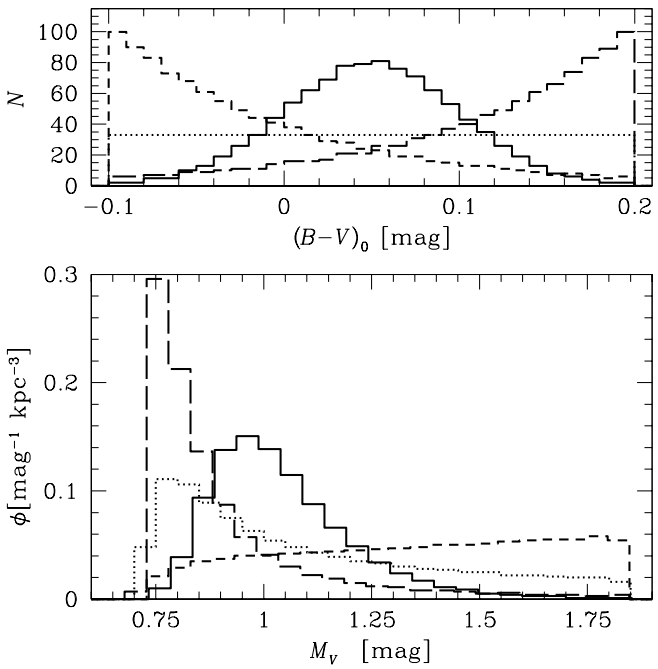

FIG. 12.—Intrinsic luminosity functions (*bottom*) recovered for four simulated intrinsic color distributions (*top*), in this case using the PSB91 M_V-color relation. The distribution of colors is the crucial element for the luminosity function.

likelihood method works by maximizing the sum of these probabilities and solving for the best-fitting luminosity function.

The density terms drop out in the maximum likelihood formalism with two notable consequences. First, the maximum likelihood method is unbiased by systematic density variations. The maximum likelihood method does not require knowledge of the halo density distribution $\rho(R, z)$; it only requires that the luminosity function is independent of position in the sampled volume. Second, the absolute normalization of the luminosity function is lost and requires a separate computation. Because stellar density varies with position in the Milky Way and because our samples are too sparse to fit the density profile directly, we compute only the *form* of the luminosity function and arbitrarily normalize the luminosity functions to unity.

4.2. *The Role of the M_V-Color Relation*

The M_V-color relations (Fig. 6) specify only how a particular color maps to a particular M_V. The distribution of colors is not at all specified by the M_V-color relation. The distribution of colors is the crucial element of the luminosity function. To illustrate this point, Figure 12 plots luminosity functions calculated for the following four *intrinsic* color distributions: (1) a uniform color distribution, (2) a Gaussian color distribution centered at $(B - V)_0 = 0.05$ with $\sigma = 0.05$ mag, and (3) exponential color distributions with scale length 0.1 mag peaking in the red and (4) the blue. Each model color distribution contains 1000 objects. For purposes of this calculation, we derive the intrinsic BHB luminosities using the PSB91 M_V-color relation, although our results are nearly identical for the other M_V-color relations in Figure 6. The bottom panel of Figure 12 shows the luminosity functions resulting from the four color distributions.

It is clear from Figure 12 that the BHB luminosity function depends dramatically on the distribution of BHB colors. Each simulated luminosity function in Figure 12 has a different shape, some with narrow distributions, others with long tails extending to faint luminosities. Moreover, the characteristic peaks of the luminosity functions vary in luminosity and total number of stars.

Even though colors are the primary indicator of BHB luminosity, we cannot compare raw distributions of colors because our field BHB stars have different luminosities and thus sample different volumes of space. To derive intrinsic properties requires knowing the luminosity function of our field BHB stars.

4.3. *The Field BHB Luminosity Function*

Figure 13 shows the luminosity function of the original Century Survey, the 2MASS-selected, and the SDSS-selected samples, determined from the observations of color, metallicity, and apparent magnitude. We use 0.2 mag wide bins to encompass any uncertainties in the M_V derivation. Luminosities are derived with the previously stated Clewley et al. (2004) relation that uses the PSB91 M_V-color relation. All three luminosity functions display the same general shape: a steep rise at bright luminosities, a peak between $0.8 < M_V < 1.0$, and a tail at faint luminosities.

We perform K-S tests to measure the likelihood that our field BHB luminosity functions are drawn from the same parent population. The K-S test applies to unbinned distributions; we thus multiply the luminosity functions (Fig. 13) by the number of objects in the samples and distribute the M_V values uniformly across each bin. The resulting likelihoods range from 37% to 57%, suggesting that our BHB samples share a common parent population. These likelihoods also mean that the bimodal distribution of luminosities in the Century Survey sample (Fig. 13*a*) is not statistically significant. Interestingly, all three samples share the same median $M_V \simeq 1.0$ mag. This agreement is rather remarkable, given the independent photometry of the three samples, and suggests that the Century Survey, 2MASS, and SDSS have consistent photometry.

Because the K-S tests suggest that our three BHB samples are drawn from the same halo population, we average the three

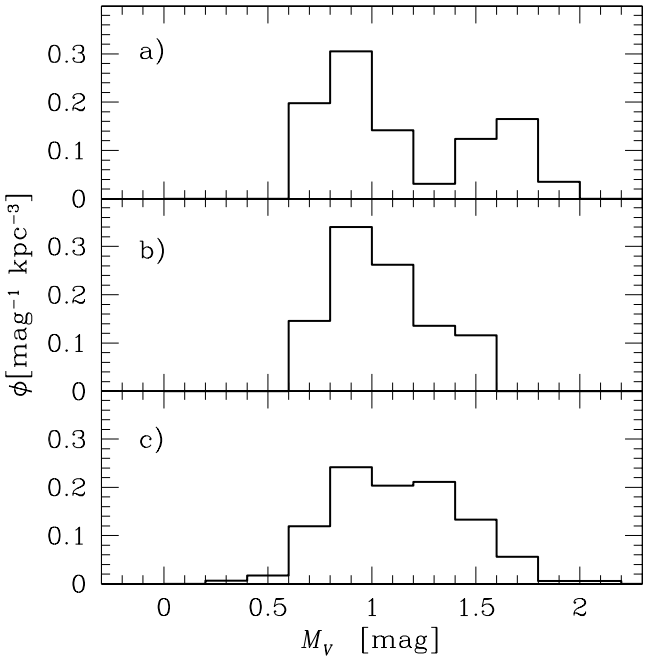

FIG. 13.—Luminosity functions of halo BHB stars in (*a*) the Century Survey sample, (*b*) the 2MASS-selected sample, and (*c*) the SDSS-selected sample. The normalization is scaled so that the areas under the curves are equal to 1.

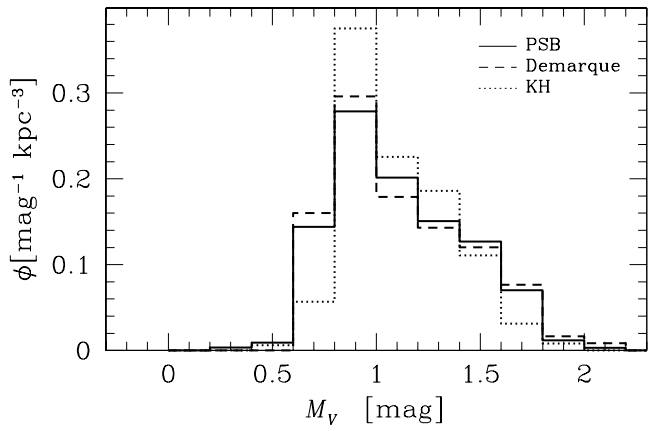

FIG. 14.—Average luminosity function of our three halo BHB star samples, calculated using (1) the empirical PSB91 M_V-color relation (*solid line*), (2) the theoretical Demarque et al. (2000) BHB models (*dashed line*), and (3) our toy model of bolometric corrections (Kenyon & Hartmann 1995) for a constant luminosity BHB star (*dotted line*).

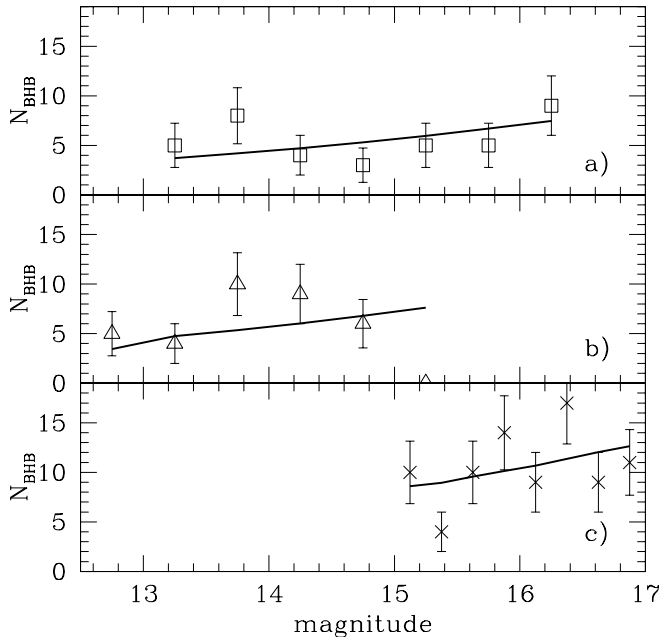

FIG. 15.—Apparent magnitude distribution of BHB stars in (*a*) the Century Survey sample, (*b*) the 2MASS-selected sample, and (*c*) the SDSS-selected sample. Extinction-corrected magnitudes are (*a*) V_0, (*b*) J_0, and (*c*) g'_0. Solid lines indicate the number of BHB stars predicted by our derived luminosity functions assuming a $r^{-2.5}$ halo density profile, normalized to the number of stars in each sample.

BHB samples to obtain a more robust measure of the field BHB luminosity function. We multiply each luminosity function in Figure 13 by the total number of BHB stars in each sample, sum the luminosity functions, and then divide the result by the grand total of BHB stars. The result is plotted as the solid histogram in Figure 14.

We recompute the luminosity functions using the M_V-color relations derived from Demarque et al. (2000) and Kenyon & Hartmann (1995). We show the results as dashed and dotted histograms, respectively, in Figure 14. Because we are interested in the shape of the luminosity function, we adjust the zero points of the M_V-color relations derived from Demarque et al. (2000) and Kenyon & Hartmann (1995) to match the zero point of the PSB91 relation. Interestingly, the theoretical Demarque et al. (2000) and empirical PSB91 curves have very similar shapes: a K-S test gives a 99% likelihood for the two samples to share a common distribution. Thus, the shapes of the theoretical and empirical M_V-color relations are similar enough to have no apparent effect on the shape of the final BHB luminosity function.

Knowledge of the BHB luminosity function allows us, in theory, to solve for the BHB density distribution. In practice, our relatively sparse samples do not provide an adequate constraint (see Fig. 15). We note that the halo power laws and scale lengths published in Siegel et al. (2002) yield reduced $\chi^2 \sim 1$ and so appear consistent with the distribution of our field BHB stars.

To check the veracity of our average BHB luminosity function, we use the luminosity function in Figure 14 (*solid histogram*) to calculate the expected apparent magnitude distributions of our BHB samples. Figure 15 plots the observed number of BHB stars in the original Century Survey, the 2MASS-selected, and the SDSS-selected samples versus extinction-corrected apparent magnitude. The error bars indicate $\sqrt{N}$ uncertainties. The solid lines in Figure 15 are the number of BHB stars predicted by the BHB luminosity function, assuming a $r^{-2.5}$ power-law density profile (Siegel et al. 2002). To set the normalization, we scale the predictions to the observed number of stars in each sample. There is good agreement in the predicted shape of the magnitude distribution and the observations. The one exception is the final 2MASS bin with $15 < J_0 < 15.5$. We attribute the observed underdensity to larger photometric errors at faint magnitudes (see Fig. 3) that scatter BHB stars out of the narrow 2MASS color-selection box, thereby reducing our completeness.

4.4. *Comparison with Globular Clusters*

An additional insight into our field BHB luminosity function is provided by comparison with globular cluster data. The purpose of this comparison is not to suggest that the halo is made of disrupted globular clusters. Rather, because all BHB stars share a common physical basis, we inquire whether they exhibit a common parent distribution of luminosities. Globular cluster BHB morphologies are known to vary widely because of differences in metallicity, main-sequence turnoff mass, and "second-parameter" effects. We expect that our wide-area surveys of the halo will sample BHB stars from the full range of BHB morphologies. We now test whether field and globular cluster BHB stars share a similar or different distribution of luminosities by comparing the shapes and median M_V values of the BHB luminosity functions.

In a brief example of the virtual observatory in action, we used the NASA ADS system (Kurtz et al. 2000) to locate suitable globular cluster data for comparison with our field BHB samples. We used the query "globular cluster color magnitude diagram" and required that there be online data associated with the paper. The first (most recent) paper that met all our requirements is the study by Hargis et al. (2004) of M12 (NGC 6218). We followed the data link to the CDS/VizieR system (Ochsenbein et al. 2000), from which the photometry data table was easily downloaded. Figure 16 shows the extinction-corrected color-magnitude diagram for M12 (*top left*). Stars on the BHB, marked as small filled squares in Figure 16, were selected by eye. M12 is relatively metal-poor, [Fe/H] ~ -1.4, similar to our halo star samples with median [Fe/H] $= -1.7$.

The inset in the top left panel of Figure 16 shows the luminosity function of BHB stars in M12. There is considerable uncertainty in the distance modulus and the metallicity of M12, with values ranging from $(m - M) = 14.22 \pm 0.11$ for [Fe/H] $= -1.14$ to $(m - M) = 13.96 \pm 0.11$ for [Fe/H] $= -1.61$. We

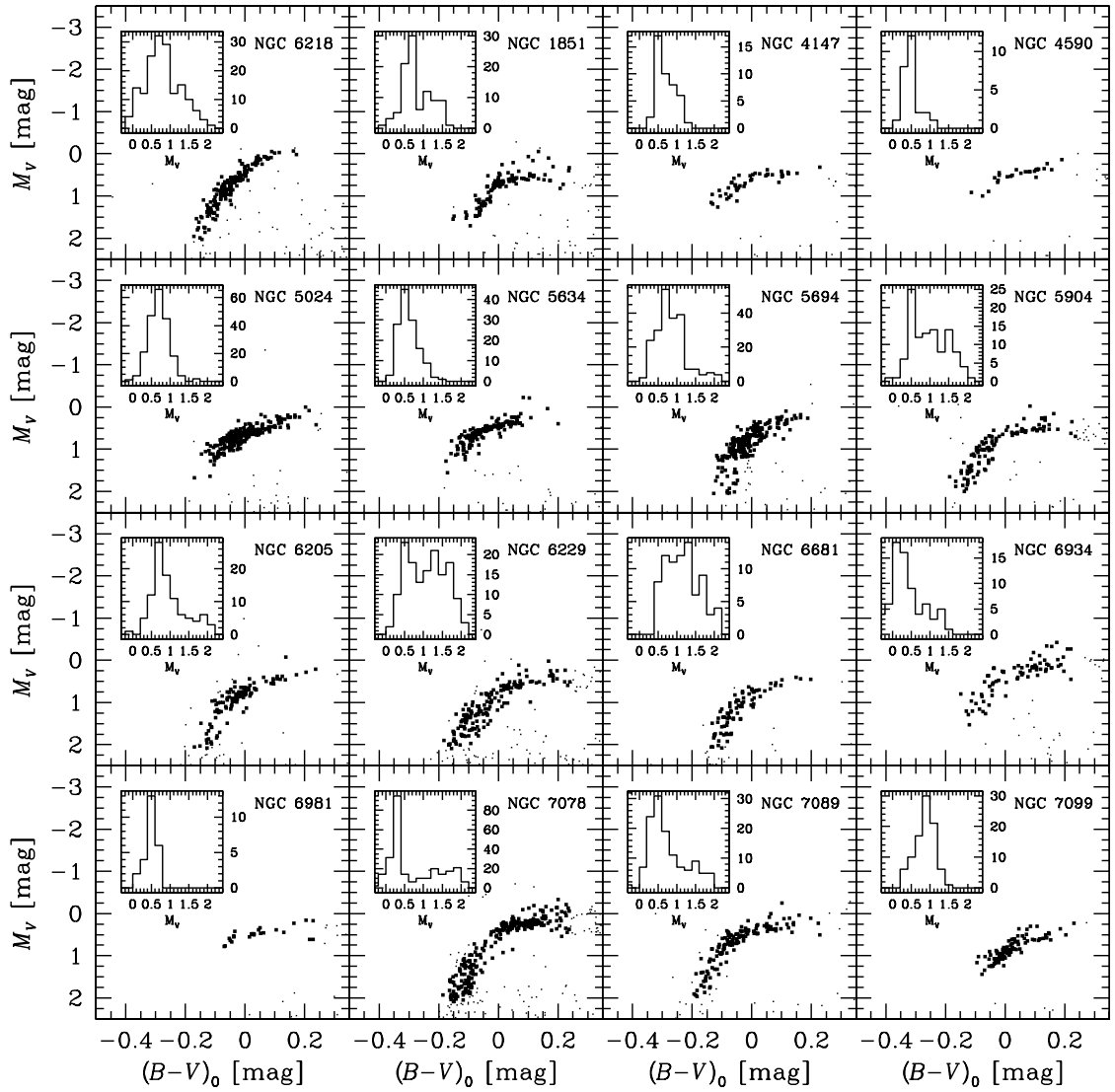

FIG. 16.—Extinction-corrected color-magnitude diagrams for M12 (NGC 6218; Hargis et al. 2004) and 15 additional globular clusters (Piotto et al. 2002). BHB stars are marked as small filled squares. The luminosity functions of the BHB stars are shown in the inset panels.

calculate absolute magnitudes using the distance modulus ($m - M$) = 14.05 ± 0.12 appropriate for [Fe/H] = −1.4 (Hargis et al. 2004) and extinction $E(B - V) = 0.19 \pm 0.02$ mag. The median extinction to our halo BHB stars, by comparison, is $E(B - V) = 0.03$ mag. The M12 BHB luminosity function has median $M_V = 0.75$, a quarter of a magnitude brighter than our field BHB samples. The disagreement in median M_V is significant only at the 1 σ level, however, since the M12 distance modulus, the M12 extinction correction A_V, and the M_V (BHB) zero point are all uncertain to ±0.1 mag.

The shape of the M12 BHB luminosity function is nearly identical to the shape of our field BHB luminosity functions. We use a K-S test as before and calculate the likelihood that the M12 and our field BHB luminosity functions are drawn from the same distribution. Because our goal is to compare the shapes of the luminosity functions, we match the median M_V of the observed and M12 samples when performing the K-S test. We find likelihoods ranging from 24% to 44% for our field BHB samples, indicating that they likely share the same distribution of BHB luminosities as the M12 BHB sample.

Piotto et al. (2002) provide online data for 74 additional globular clusters that we use for further comparison. The data come from *Hubble Space Telescope* F439W and F555W imaging from which Piotto et al. (2002) derive dereddened B and V magnitudes. Because *Hubble Space Telescope* targeted the centers of the globular clusters, not all of the color-magnitude diagrams are as well sampled as the Hargis et al. (2004) M12 data. One-third of the Piotto et al. (2002) globular clusters have horizontal branches that are nonexistent or too sparsely populated to provide a meaningful comparison with our BHB samples. Of the remaining 51 globular clusters, we select the 15 with $E(B- V) < 0.1$ mag to minimize uncertainties in extinction. These 15 globular clusters span the range of metallicity $-2.3 <$ [Fe/H] < -1.2.

Figure 16 shows the extinction-corrected color-magnitude diagrams for the 15 globular clusters from Piotto et al. (2002). We calculate absolute magnitudes using the distance moduli and extinction values given by Piotto et al. (2002). Interestingly, each of the 15 globular clusters has a different median BHB M_V than our BHB samples. There is no correlation with globular cluster metallicity. The average globular cluster median BHB luminosity is $M_V = 0.7 \pm 0.25$ mag. Although a 0.3 mag difference from our BHB samples is not formally significant, we expected better agreement when averaging over this set of globular clusters. In Paper I, we noticed a similar ~0.3 mag discrepancy between our

absolute magnitudes and the theoretical calculations for the zero-age horizontal branch. For example, the Demarque et al. (2000) model discussed here (Fig. 6) is 0.1 mag brighter than the PSB91 relation. If the zero point of our M_V(BHB) relation is in error by 0.3 mag, then our BHB stars are 14% more distant than our current estimates. Given the strong dependence of BHB luminosity on color, it may be worth revisiting the PSB91 analysis and their zero point.

The *shape* of the Piotto et al. (2002) globular cluster BHB luminosity functions are in good agreement with our field BHB luminosity functions. The globular cluster BHB stars are marked as small filled squares in Figure 16. We select BHB stars by color and magnitude cuts, imposing the same limits, $(B-V) < 0.24$ mag and $M_V < 2.1$ mag, as for our samples. The insets in Figure 16 show the luminosity functions of globular cluster BHB stars. We perform K-S tests on the shapes of the luminosity functions as before, first matching the median M_V of the globular cluster BHB stars to our BHB samples. The likelihoods that the BHB stars are drawn from the same distribution range from 20% to 80%, with the exception of two globular clusters. NGC 6229 and NGC 7078 (M15) have significant extended horizontal branches and thus a much broader distribution of BHB luminosities than our field BHB samples. The K-S test yields a 10% likelihood for NGC 6229, which would only allow a very marginal rejection of the null hypothesis of a common parent distribution. A 1% likelihood is obtained for NGC 7078, indicating that its luminosity distribution is not consistent with our field BHB samples. We note that the metallicities of NGC 6229 and NGC 7078 are $[\mathrm{Fe/H}] = -1.43$ and -2.25, respectively.

Of the 16 globular clusters displayed in Figure 16, 14 (88%) have luminosity functions consistent in shape with our field BHB luminosity functions. Thus, under the assumption that the M_V-color relation is intrinsic to stars on the BHB, we find that field BHB stars in the halo and BHB stars in globular clusters with BHBs appear to share a common distribution of luminosities. The exception to this conclusion are globular clusters with significant extended BHBs; we do not see large numbers of extended BHB stars with $(B-V)_0 < -0.1$ in our samples. In the future, it would be useful to compare our field BHB luminosity function with dwarf spheroidal galaxies and open clusters.

5. CONCLUSIONS

We extend the Century Survey Galactic Halo Project based on a new 175 deg^2 spectroscopic survey for BHB stars. We make use of the 2MASS and SDSS photometric catalogs and show that the 2MASS and SDSS color-selection is 38% and 50% efficient, respectively, for BHB stars. The 2MASS selection for BHB stars is 65% *complete* (Brown et al. 2004) but is likely to be worse in the magnitude range $15 < J_0 < 15.5$ because of large photometric errors scattering BHB stars out of the narrow color selection range. The SDSS completeness for BHB stars is also magnitude dependent and appears to drop to 50% in the magnitude range $15 < g'_0 < 15.5$ because of saturation problems.

We analyze the global properties of the original Century Survey, the 2MASS-selected, and SDSS-selected BHB stars and find them consistent with a predominantly halo population. The median metallicity of the BHB stars is $[\mathrm{Fe/H}] = -1.7$. K-S tests indicate that the BHB samples share a common metallicity distribution. The velocity dispersion of the BHB stars is 108 km s^{-1}. The mean Galactic rotation of the BHB stars 3 kpc $< |z| <$ 15 kpc is -4 ± 30 km s^{-1}. Our samples also include a likely runaway B7 star 6 kpc below the Galactic plane.

The luminosity of a BHB star is primarily temperature (color) dependent. The shape of the M_V-color relation is due to the physics of BHB stars. We show that the shape of the PSB91 observationally derived M_V-color relation corresponds to the Demarque et al. (2000) theoretical BHB models and to the Kenyon & Hartmann (1995) bolometric corrections. We derive luminosities to our field BHB stars under the assumption that the M_V-color relation is intrinsic to stars on the BHB.

The M_V-color and M_V-metallicity relations impose selection biases on a flux-limited survey. A flux-limited survey samples hot BHB stars with $(B-V)_0 = -0.1$ to 64% of the depth for BHB stars with $(B-V)_0 = +0.1$. Similarly, a flux-limited survey samples metal-rich BHB stars with $[\mathrm{Fe/H}] = -1$ to 82% of the depth for metal-poor BHB stars with $[\mathrm{Fe/H}] = -3$.

We calculate the luminosity function for our field BHB star samples using the maximum likelihood method of Efstathiou et al. (1988), a technique that is nonparametric and unbiased by density inhomogeneities. The luminosity function for field BHB stars is characterized by a steep rise at bright luminosities, a peak between $0.8 < M_V < 1.0$, and a tail at faint luminosities. We show that the luminosity function is not determined by the shape of the M_V-color relation but rather the way this relation is populated. We compare our luminosity functions with the BHB luminosity functions derived from 16 different globular clusters. K-S tests indicate that globular clusters with BHBs, but not globular clusters with significant extended BHBs, have similar distributions of BHB star luminosities as our field BHB star samples.

We plan to analyze our samples of BHB stars for velocity and spatial substructure. Knowing the global properties and luminosity function of the BHB stars is an important step in this analysis. Furthermore, knowing the 2MASS and SDSS color-selection efficiencies and completenesses for BHB stars helps to guide our continuing observations. The eventual goal of our Galactic Halo Project is to identify star streams in the halo and thus to test the hierarchical picture for galaxy formation.

We thank Perry Berlind and Mike Calkins for their dedicated observing at the Whipple 1.5 m Tillinghast Telescope. We thank P. Demarque and Y. Lee for correspondence concerning the BHB M_V-color relation. We thank the referee for a careful and thoughtful report. This project makes use of NASA's Astrophysics Data System bibliographic services. This project makes use of data products from the Two Micron All Sky Survey, which is a joint project of the University of Massachusetts and the Infrared Processing and Analysis Center, Caltech, funded by NASA and the NSF. This project makes use of data products from the Sloan Digital Sky Survey, which is managed by the Astrophysical Research Consortium for the Participating Institutions. Funding for SDSS has been provided by the Sloan Foundation, the Participating Institutions, NASA, the NSF, the US Department of Energy, the Japanese Monbukagakusho, and the Max Planck Society. This work was supported by W. Brown's CfA Fellowship. T. C. B. acknowledges partial support of this work from grants AST 04-06784 and PHY 02-16783, Physics Frontier Centers/JINA: Joint Institute for Nuclear Astrophysics, awarded by the NSF.

APPENDIX

DATA TABLES

Tables 2 and 3 list the photometric and spectroscopic measurements for the 2MASS-selected and SDSS-selected samples. The tables contain 257 entries and include every 2MASS- and SDSS-selected object except for the 27 G-type stars in the SDSS-selected sample. The SDSS-selected G-types have erroneous

TABLE 2
PHOTOMETRY

ID (1)	$\alpha_{J2000.0}$ (2)	$\delta_{J2000.0}$ (3)	J_0 (mag) (4)	g'_0 (mag) (5)	$E(B-V)$ (mag) (6)	$BV0$ (mag) (7)	BHB (8)
CHSS 1598	03 41 13.2	00 48 37	...	15.27 ± 0.013	0.09	−0.03	0
CHSS 1599	03 43 57.6	00 08 57	...	15.11 ± 0.020	0.09	0.15	0
CHSS 1600	23 00 20.9	−00 17 10	14.22 ± 0.026	...	0.05	0.16	0
CHSS 1601	23 02 10.7	−01 01 10	14.65 ± 0.038	...	0.05	−0.01	1
CHSS 1602	23 03 58.3	−01 08 12	13.59 ± 0.030	...	0.04	−0.02	1

NOTE.—Table 2 is presented in its entirety in the electronic edition of the *Astronomical Journal*. A portion is shown here for guidance regarding its form and content.

TABLE 3
SPECTROSCOPIC AND STELLAR PARAMETERS

ID (1)	KP (2)	HP2 (3)	GP (4)	v_{radial} (km s^{-1}) (5)	Type (6)	T_{eff} (K) (7)	log g (cm s^{-2}) (8)	[Fe/H] (9)	Distance (kpc) (10)	M_V (mag) (11)
CHSS 1598	1.97	11.00	0.89	41.0 ± 27.6	22.0 ± 1.0	8413	4.99	−0.17	5.73	1.28
CHSS 1599	1.72	10.11	1.38	−13.9 ± 26.1	31.6 ± 2.6	8243	4.99	−0.53	1.93	3.60
CHSS 1600	1.90	10.07	0.81	−44.4 ± 11.0	21.2 ± 1.0	8208	4.99	−0.29	2.75	2.09
CHSS 1601	0.47	10.91	0.05	−92.4 ± 10.0	21.6 ± 1.2	9111	3.50	−1.77	4.67	1.23
CHSS 1602	0.31	10.91	0.27	9.9 ± 9.8	21.6 ± 1.2	9095	3.50	−1.49	2.65	1.33

NOTE.—Table 3 is presented in its entirety in the electronic edition of the *Astronomical Journal*. A portion is shown here for guidance regarding its form and content.

photometry, likely due to saturation problems in the SDSS. Tables 2 and 3 are presented in their entirety in the electronic edition of the *Astronomical Journal*. Portions of the tables are shown here for guidance regarding their format and content.

Table 2 summarizes the photometry. Column (1) is our identifier. The designation CHSS stands for Century Halo Star Survey and is chosen to be unique from previous surveys. Column (2) is the J2000.0 right ascension in hours, minutes, and seconds. Column (3) is the J2000.0 declination in degrees, arcminutes, and arcseconds. Column (4) is the 2MASS extinction-corrected J_0 magnitude for the 2MASS-selected stars. Column (5) is the SDSS extinction-corrected g'_0 magnitude for the SDSS-selected stars. Column (6) is the $E(B-V)$ reddening value from Schlegel et al. (1998). Column (7) is the $BV0$ color predicted from 2MASS or SDSS photometry and Balmer line strengths (Brown et al. 2003). Column (8) is the BHB classification: 1 if the star is BHB, 0 if it is not.

Table 3 summarizes the spectroscopic and stellar parameters. Column (1) is our identifier. Column (2) is the KP (Ca II) index. Column (3) is the HP2 (Hδ) index. Column (4) is the GP (G-band) index. Column (5) is the heliocentric radial velocity in km s^{-1}. Column (6) is the spectral type, where B0 = 10, A0 = 20, F0 = 30, and so forth. Column (7) is the effective temperature in K. Column (8) is the base-10 logarithm of the surface gravity in cm s^{-2}. Column (9) is the metallicity given as the logarithmic [Fe/H] ratio relative to the Sun. Column (10) is the estimated distance in kpc. Column (11) is the absolute M_V magnitude corrected for reddening, given the estimated distance.

REFERENCES

Abazajian, K., et al. 2003, AJ, 126, 2081
———. 2004, AJ, 128, 502
Allende Prieto, C. 2003, MNRAS, 339, 1111
Arnold, R., & Gilmore, G. 1992, MNRAS, 257, 225
Beers, T. C., Rossi, S., Norris, J. E., Ryan, S. G., & Shefler, T. 1999, AJ, 117, 981
Bowers, R. L., & Deeming, T. 1984, Astrophysics: Stars, Vol. 1 (Boston: Jones & Bartlett)
Brown, W. R., Allende Prieto, C., Beers, T. C., Wilhelm, R., Geller, M. J., Kenyon, S. J., & Kurtz, M. J. 2003, AJ, 126, 1362 (Paper I)
Brown, W. R., Geller, M. J., Kenyon, S. J., Beers, T. C., Kurtz, M. J., & Roll, J. B. 2004, AJ, 127, 1555
Carney, B. W., Latham, D. W., & Laird, J. B. 2005, AJ, 129, 466
Chiba, M., & Beers, T. C. 2000, AJ, 119, 2843
Clementini, G., Gratton, R., Bragaglia, A., Carretta, E., Di Fabrizio, L., & Maio, M. 2003, AJ, 125, 1309
Clewley, L., Warren, S. J., Hewett, P. C., Norris, J. E., & Evans, N. W. 2004, MNRAS, 352, 285
Clewley, L., Warren, S. J., Hewett, P. C., Norris, J. E., Peterson, R. C., & Evans, N. W. 2002, MNRAS, 337, 87
Cox, A. N. 2000, Allen's Astrophysical Quantities (4th ed.; New York: Springer)
Cutri, R. M., et al. 2003, 2MASS All Sky Catalog of Point Sources (Pasadena: IPAC)
Dehnen, W., & Binney, J. J. 1998, MNRAS, 298, 387
Demarque, P., Zinn, R., Lee, Y., & Yi, S. 2000, AJ, 119, 1398
Efstathiou, G., Ellis, R. S., & Peterson, B. A. 1988, MNRAS, 232, 431
Fabricant, D., Cheimets, P., Caldwell, N., & Geary, J. 1998, PASP, 110, 79
Frenk, C. S., & White, S. D. M. 1980, MNRAS, 193, 295
Gilmore, G., Wyse, R. F. G., & Norris, J. E. 2002, ApJ, 574, L39
Gould, A., & Popowski, P. 1998, ApJ, 508, 844
Green, E. M., Demarque, P., & King, C. R. 1987, The Revised Yale Isochrones and Luminosity Functions (New Haven: Yale Obs.)
Hargis, J. R., Sandquist, E. L., & Bolte, M. 2004, ApJ, 608, 243
Kenyon, S. J., & Hartmann, L. 1995, ApJS, 101, 117
Kinman, T. D., Bragaglia, A., Cacciari, C., Buzzoni, A., & Spagna, A. 2005, Proc. *GAIA* Symp.: The Three Dimensional Universe with *GAIA*, ed. C. Turon, K. S. O'Flaherty, & M. A. C. Perryman (ESA SP-576; Noordwijk: ESA), 175
Kinman, T. D., Suntzeff, N. B., & Kraft, R. P. 1994, AJ, 108, 1722
Kurtz, M. J., Eichhorn, G., Accomazzi, A., Grant, C. S., Murray, S. S., & Watson, J. M. 2000, A&AS, 143, 41
Layden, A. C., Hanson, R. B., Hawley, S. L., Klemola, A. R., & Hanley, C. J. 1996, AJ, 112, 2110
Lejeune, T., Cuisinier, F., & Buser, R. 1998, A&AS, 130, 65
Majewski, S. R. 1992, ApJS, 78, 87
Majewski, S. R., Munn, J. A., & Hawley, S. L. 1996, ApJ, 459, L73

Martin, J. C., & Morrison, H. L. 1998, AJ, 116, 1724
Norris, J. E., & Hawkins, M. R. S. 1991, ApJ, 380, 104
Ochsenbein, F., Bauer, P., & Marcout, J. 2000, A&AS, 143, 23
Pier, J. R. 1983, ApJS, 53, 791
Piotto, G., et al. 2002, A&A, 391, 945
Preston, G. W., Beers, T. C., & Shectman, S. A. 1994, AJ, 108, 538
Preston, G. W., Shectman, S. A., & Beers, T. C. 1991, ApJ, 375, 121 (PSB91)
Preston, G. W., & Sneden, C. 2000, AJ, 120, 1014
Schlegel, D. J., Finkbeiner, D. P., & Davis, M. 1998, ApJ, 500, 525
Siegel, M. H., Majewski, S. R., Reid, I. N., & Thompson, I. B. 2002, ApJ, 578, 151
Sirko, E., et al. 2004a, AJ, 127, 899
Sirko, E., et al. 2004b, AJ, 127, 914
Sommer-Larsen, J., Christensen, P. R., & Carter, D. 1989, MNRAS, 238, 225
Spagna, A., Cacciari, C., Drimmel, R., Kinman, T., Lattanzi, M. G., & Smart, R. L. 2003, in ASP Conf. Ser. 298, *GAIA* Spectroscopy: Science and Technology, ed. U. Munari (San Francisco: ASP), 137
Stoughton, C., et al. 2002, AJ, 123, 485
Wilhelm, R., Beers, T. C., & Gray, R. O. 1999a, AJ, 117, 2308
Wilhelm, R., Beers, T. C., Sommer-Larsen, J., Pier, J. R., Layden, A. C., Flynn, C., Rossi, S., & Christensen, P. R. 1999b, AJ, 117, 2329
Yanny, B., et al. 2000, ApJ, 540, 825
York, D. G., et al. 2000, AJ, 120, 1579